A Microfluidic- Colorimetric Sensor for Continuous Monitoring of Reactive Environmental Chemicals

Rui Wang, Amlendu Prabhakar, Rodrigo A. Iglesias, Xiaojun Xian, Xiaonan Shan, Francis Tsow, Erica S. Forzani, and Nongjian Tao

***Abstract*— Colorimetry is a powerful sensing principle that detects a target analyte based on a reaction-induced color change. The approach can be highly sensitive and selective when a sensing material that reacts specifically with the analyte is found, but the specific reaction is usually accompanied by slow recovery and irreversibility, making continuous monitoring of air quality difficult. Consequently, colorimetry is often one-time only and single point measurement. To overcome the difficulty, the present work reports a combined microfluidic and colorimetric approach that measures time evolution of a color gradient along a microfluidic channel via a Complementary Metal Oxide Semiconductor (CMOS) imager. The change of the color gradient provides continuous monitoring of the analyte concentration over many hours, and the principle and capability of the approach is demonstrated by theoretical simulation, and experimental validation with real samples.**

***Index Terms*— Environmental sensors, chemical sensors, colorimetry, nitrogen oxides, ozone.**

I. Introduction

MONITORING of reactive chemicals, such as nitrogen oxides (NO_x) and ozone, in air is critical for environmental protection and studies of problems, such as traffic related pollution[1], acid rain[2], ozone layer depletion[3] and photochemical smog[4]. These pollutants can cause serious health problems[5], especially in children and people with sensitive respiratory diseases[5, 6]. In January, 2010, U.S. Environmental Protection Agency (EPA) raised the National Ambient Air Quality Standard (NAAQS), and set a new hourly NO_2 standard to 100 ppbV while retaining existing annual average standard of 53ppbV[7]. To date the most commonly used detection method for NO_x is based on fixed air quality monitoring stations[8] using equipment based on chemiluminescence detection combined with catalytic reduction of NO_2[9]. The chemiluminescence equipment is the gold standard for NO_x measurement, but it requires a powerful vacuum pump and *in situ* ozone generation, which demands high power, volume and cost,[10] and further generates an air pollutant.

In order to assess air pollutants with high spatial and temporal resolution at personal level and in microenvironments, it is necessary to develop a low cost, low power, large dynamic range, and miniaturized device that can provide real time and continuous monitoring of air pollutants.

Colorimetric method detects an analyte based on a color change induced by a specific reaction of the analyte with a sensing material. The method is widely used for its simplicity, high sensitivity, and selectivity. Recently, colorimetric detection has been successfully used in an electronic nose fashioned to provide a rather universal platform for identification of complex compounds[11]. The specific reaction is responsible for the high specificity and selectivity, but it also leads to slow recovery and irreversibility, making it difficult for continuous monitoring of toxic chemicals in air over a long time. For these reasons, colorimetric method is often for one-time use only.

Here we present a colorimetric detection method that can sensitively, continuously, and selectively monitor toxic chemicals. It combines the concept of colorimetric sensor with microfluidic and CMOS imaging (e.g., webcam) techniques (**Fig. 1**). The sample air flows through a microchannel coated with a sensing material specific for a target analyte, and the reaction of the analyte with the sensing material leads to a change in color along the microfluidic channel from the inlet to the outlet, which is monitored in real time with the CMOS imager. The color in the region near the inlet changes first because this region reacts with and consumes most of the analytes. Consequently, a color gradient, reflecting the concentration gradient of the reaction products, develops near the inlet. As the reaction consumes the sensing material near the inlet, the color gradient moves along the channel towards the outlet, and a change of the color gradient over time recorded with the CMOS provides a real time and continuous monitoring of the analyte. An image processing routine follows the color gradient along the channel and determines the analyte concentration. Furthermore, due to the presence of "downstream" fresh sensing material, the approach facilitates

Manuscript received 5/2, 2011. This work was supported by NSF under Grant BS123456 and NIH/NIEHS under Grant U01 ES016064-02.

R.Wang, A.Prabhakar, R.Iglesias, X.Xian, X.Shan, F.Tsow, E.Forzani and N. Tao are with the Biodesign Institute. Tao and Forzani also with Ira A Fulton Schools of Engineering, Arizona State University, Tempe, AZ 85287-5801 USA (e-mail: rui.wang.2@asu.edu; amlendu.prabhakar@asu.edu; Rodrigo.Iglesias@asu.edu; Xiaojun.Xian@asu.edu; xshan2@asu.edu; tsing.tsow@asu.edu; Erica.Forzani@asu.edu; njtao@asu.edu).

continuous detection without losing sensitivity, and maximizes the dynamic range of the detection. We have carried out theoretical simulation and analytical experiments to validate the new detection approach, and tested real environmental samples to demonstrate its usability.

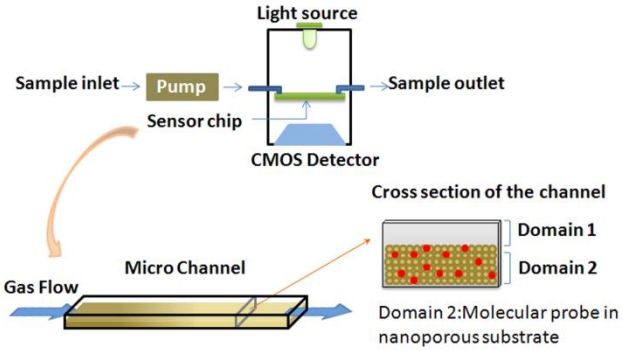

Fig. 1. Schematics of the experimental setup and the sensing channel.

II. Experiment and Simulation Methods

A. Microfluidic channel and flow system

The microfluidic channel with a dimension of 150 μm (depth) × 1 mm (width) × 7 mm (length) is fabricated on an acrylic substrate (U.S. Plastic Corp.) using CNC machine. The acrylic channel is uniformly coated with silica gel solution (Whatman Ltd., P/N:4410221). The silica gel solution is prepared in an aqueous solution (silica gel: water =1:7) of a NO_2 sensing material (see below). After coating, the silica gel channel is dried in vacuum for half an hour at room temperature. The silica gel is chosen because of its porous structure, which provides high loading capacity of the sensing element and excellent sensitivity for monitoring environmental NO_2.

B. Sensing material for NO_2

The sensing material is o-phenylenediamine (PDA) (Sigma-Aldrich, Inc.), a sensitive and selective material for NO_2 detection[12]. PDA is colorless and turns into yellow upon reaction with NO_2. The reaction is irreversible and has an intrinsic fast kinetics with a colored phenazine derivative as product, which allows NO_2 detection and quantification (see below)[12]. In addition, since PDA has a relatively high oxidation potential, it offers excellent selectivity against other common interferences present in ambient air. Previous studies by us showed that the sensing material is highly selective against common interfering chemicals, including SO_2, CO, CO_2, NH_3, H_2S, acetone, and ethanol[12]. However, ozone, a strong oxidant, appears to interfere with the detection. To minimize this interference, an ozone scrubber filter based on molybdenum oxide derivative (2B Technologies, Boulder, Co.) is used to remove ozone. This material can also adsorb NO_2 but with much lower effiency. The mass and packing of the ozone scrubber is optimized to remove 100% ozone while preserving 90% of NO_2. Humidity, also an interference, is removed by a nafion tubing(Perma Pure, LLC). In order to measure total NO_x ($NO + NO_2$), an additional homemade filter with sodium permanganate particles (Purafil^{TM}) packed in a glass tube is used to oxidize NO to NO_2 and enable the NO detection concurrently with NO_2.

C. Optical detection

A device based on the microfluidic and colorimetric concept is fabricated (**Fig. 1.**). A white LED (LEDtrnics. Inc.) connected to a constant current source is used as light source to illuminate the microfluidic channel. A CMOS detector (Logitech, Inc.) is used to record videos of the channel area with a frame rate of 5 frames per second (fps). Nineteen regions along the channel are chosen for detailed analysis of reaction kinetics. A reference region outside the channel is selected for calculating the absorbance using a Matlab program. The Matlab program deconvolutes the color information, and calculates the average intensity values (I) of red (R), green (G), and blue (B) components for each of the 20 regions (19 sampling regions inside the channel and 1 reference region outside the channel), and then determines the absorbance change for each sampling region inside the channel using the following equation:

$$\Delta A = -\log(I_{sampling}(t)/I_{reference}(t)) - \text{constant} \qquad (1)$$

where $I_{sampling}$ and $I_{reference}$ are R or G or B intensity values, and "constant" is the initial absorbance value before the analyte is brought into the channel. The absorbance change is used to determine the analyte concentration using procedures described in later sections. We note that the reference region allows us not only to calculate the absorbance changes, but also to correct drifts from the light source. UV-visible spectrum previously showed that the reaction product between PDA and NO_2, produces the largest change in the blue component due to a maximum absorbance at 380-390 nm[12]. For this reason, the absorbance changes are calculated from the blue component of the CMOS imager.

D. Sample collection and measurement

For lab-based testing, air samples with different NO_2 concentrations are prepared in Tedlar bags. To obtain samples with different NO_2 concentrations, varying amounts of 50 ppmV standard NO_2 gas purchased from Praxair, Inc. are injected into and diluted in 4L clean Tedlar bags. For testing real samples, the gas samples are first collected into Tedlar bags using a pump with a homemade particle filter (polyester fibers) at the inlet, and then taken back to the lab for measurement. A miniature pump (Schwarzer Precision, Co) with a fixed flow rate of 40ml·min^{-1} is used to introduce the air sample into the microchannel. All the gas samples are handled with caution.

E. Simulation method

To numerically simulate the chemical reaction kinetics and mass transport of the analytes along the fluidic channel[13], we divide the channel into two domains, shown by the cross sectional view of the channel in Fig. 1. The upper domain (domain 1) is the space between the top of silica gel layer and the ceiling of the channel, in which sampled air containing the analyte flows, and the lower domain (domain 2) is the silica

gel layer containing the sensing material, PDA. We first calculate the velocity field (linear velocity distribution) of the gas sample along the channel by solving momentum transport equations for each domain with appropriate boundary conditions[14]. In the calculation of the velocity field, we neglect the reaction of the analyte in domain 2. This approximation is reasonable as long as the analyte concentration is low compared to the concentration of other air components (typically ~ 20% oxygen and 80% nitrogen), so that the reaction in domain 2 does not change the distribution of the velocity field.

When simulating the velocity field of the analyte it is decoupled from the diffusion, convection and reaction of the system in the simulation. In domain 1, we assume that the air samples are incompressible Newtonian fluids. This is a valid assumption because the flow velocity is much smaller than the velocity of sound in air[15]. The incompressible Navier-Stokes equation used in this domain is written as

$$\rho(\partial u/\partial t)+\rho(u\cdot\nabla)u=\nabla\cdot[-pI+\eta(\nabla u+(\nabla u)^T)] \quad (2)$$

where u is the flow velocity, p is the pressure, ρ is the density (1 kg·m^{-3}) and η is the dynamic viscosity (1.78×10^{-5} Pa·s)[16] at 300 K.

We model domain 2, where the silica gel is present, as a porous medium, in which Brinkman equation applies[17]. Note that the equation is an extension from Darcy's law, and given by

$$(\eta/\kappa)u=\nabla\cdot[-pI+1/\varepsilon_p\{\eta(\nabla u+(\nabla u)^T-2\eta/3(\nabla\cdot u)I)\}] \quad (3)$$

where ε_p is the porosity of silica gel (0.76) and κ is the permeability (1×10^{-2} m^2). The porosity is calculated from the channel preparation process and permeability is an estimate from the experiment.

The boundary conditions are defined as follows:

Inlet: U_0 = 1.5 m·s^{-1}, which is normal inflow velocity.

Outlet: p_0 = 0 kPa, which means no viscous stress at the end of the channel.

Interface between domains 1 and 2: continuity conditions.

All the other boundaries: velocity **u** equals to 0.

Upon solving the equations (2) and (3), the velocity of the gas sample is simulated using Comsol 4.0.

After determining the velocity field, we use the information to solve the reaction of the analyte in domain 2. The reaction can be denoted as: $c(g)+n(s)\rightarrow p(s)$, where c is the analyte concentration, n is the density of binding sites available for the reaction and p is the product concentration generated by the reaction.

In domain 1, only the analyte is present, and no reaction takes place. The concentration distribution of the analyte in domain 1 is described by the following convection-diffusion equation:

$$\partial c/\partial t=V\cdot\nabla c+D\nabla^2 c \quad (4)$$

where V is the velocity of the air sample in domain 1, which is pre-determined in the first step, D is the diffusion coefficient of the analyte in domain 1[18], which is equal to 1.3×10^{-5}m^2·s^{-1}.[19]

In domain 2, the reaction takes place, which changes the concentrations of the analyte (c), binding sites (n), and reaction product (p), and an additional term representing the reaction is included in the convection-diffusion equation. In addition, a rate equation relating the change of the binding sites and the analyte concentration is also considered. The equations describing these processes are as follows:

$$\partial c/\partial t=V\cdot\nabla c+D\nabla^2 c-kcn \quad (5)$$

$$\partial n/\partial t=-kcn \quad (6)$$

where k is the reaction rate coefficient equal to 2 m^3·mol^{-1}·s^{-1}, and D is the diffusion coefficient in domain 2 (equal to D in domain 1). Since diffusion is relatively small compared to convection, it has small effect on sensing. The k is obtained by comparison of simulation and experimental results obtained with a sensing surface with no mass transport limitations.

The boundary conditions are defined as follows:

Inlet: c(t) = f(t), which is determined by the analyte concentration of the air sample, a quantity to be measured.

Outlet: c=0, which means the convective flux is the dominant component at the outlet.

Interface between domains 1 and 2: continuity boundary condition is assumed.

All the other boundaries: $-D\nabla c+cV$, the inward flux, is set to zero, which is valid as long as the system is closed (sealed) at these boundaries.

Solving equations (4)-(6), together with the boundary conditions defined above, allows us to determine c(x,t) and n(x,t) along the channel using Comsol 4.0. The color change is proportional to p(x,t), the reaction product distribution, which is directly related to n(x,t) by p(x,t) = n_0 - n(x,t), where n_0 is the initial reaction sites concentration. In other words, the depletion of the reaction sites equals the generation of the reaction product.

III. Results and Discussion

A. Simulation

We described the basic principle of the combined microfluidic and colorimetric detection in the introduction. To fully evaluate the principle, we carried out theoretical simulation by solving the transport and reaction rate equations with proper initial and boundary conditions using the method described above. From the simulation, direct observation of the color progression can be obtained. Fig. 2. shows the simulation results of the sensor when exposed to clean air for 5 minutes, followed by exposure to 1 ppmV NO_2 for 0.5, 1.0 and 1.5 hours, respectively, and to clean air again for 5 minutes. The concentration profile of unreacted binding sites along the channel and its evolution with time is shown in Fig. 2A. We note that due to symmetry with respect to the x-axis, only a half of the width was simulated. At t=0.5 hr, a small portion of the channel near the inlet begins to react, but the region near the outlet remains unreacted (same color). At t=1.0

hr, more color changes can be seen along the channel even in the region close to outlet. At t=1.5 hr, the binding sites near the inlet are closer to full depletion (saturation), but the remaining portion, especially regions near the outlet remain unsaturated.

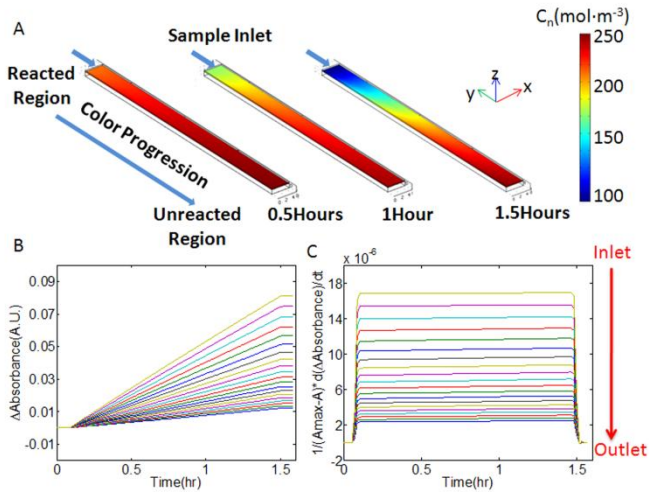

Fig. 2. A) Concentration profile of unreacted binding sites along the channel when exposed to clean air for 5 minutes, followed by exposure of 1ppmV NO2 for 0.5, 1 and 1.5 hours, respectively, and clean air for 5 additional minutes. The concentration profile also represents the color progression or optical absorbance along the channel. B) The absorbance changes over time for different regions of the channel (represented in different colors). C) After applying equation (9), each region provides the concentration profile at different amplitudes. Different colors represent different regions.

The color changes shown in fig. 2A reflect the concentration changes of the binding sites along the channel, which is proportional to the absorbance change. So we can obtain the relative absorbance change, which can be experimentally measured using the following equation:

$$\Delta A/\Delta A_{\max} = (n_0 - n(t))/n_0 \qquad (7)$$

where the denominator n_0 is proportional to the maximum absorbance change ($n_o = p_{max}$, $n_o \propto \Delta A_{max}$) and taken into account for normalization of optical path length and extinction coefficient of *p*. Fig. 2B plots the relative absorbance change vs. time at different locations along the channel (represented by solid lines with different colors). The plot shows a linear response to NO_2 with time. It also shows that the relative absorbance changes the most at the inlet (largest slope), and least at the outlet (smallest slope).

A more direct way to relate the color pattern to the analyte concentration in air is to re-express equation (6) as

$$c(x,t) = -\frac{1}{kn}\cdot\frac{dn}{dt} = \frac{1}{k(n_0 - p)}\frac{dp}{dt} \qquad (8)$$

where $p = n_0 - n$, is used to express n in terms of p. Since the absorbance change, ΔA, is proportional to p, and equation (8) becomes

$$c(x,t) = -\frac{1}{kn}\cdot\frac{dn}{dt} = \frac{1}{k(\Delta A_{\max} - \Delta A)}\frac{d\Delta A}{dt}, \qquad (9)$$

where ΔA_{max} is the maximum absorbance. At the inlet, $c|_{inlet} = f(t)$, the analyte concentration in air sample, so that $\frac{1}{k(\Delta A_{\max} - \Delta A)}\frac{d\Delta A}{dt}|_{inlet}$ measures the analyte concentration. Numerical simulation also shows that the time profile of $\frac{1}{k(\Delta A_{\max} - \Delta A)}\frac{d\Delta A}{dt}$ at any location along the channel is proportional to the analyte concentration (**Fig. 2C**). The simulation confirms that one can determine the analyte concentration by employing a microfluidic channel and a CMOS imager. The imager monitors the color change along the entire channel so that one can focus on the regions with unreacted sites, thus avoiding saturation problem in the conventional colorimetric sensors without sacrificing sensitivity. This approach maximizes dynamic range and lifetime, and allows for continuous monitoring of reactive analytes.

B. Experimental validation

In addition to theoretical simulation, we have carried out systematic experiments to further validate the microfluidic-colorimetric detection principle. As described in the experimental section, the sensor chip consists of a microfluidic channel with its bottom surface coated with a layer of PDA-modified silica gel. We connect the inlet of the microfluidic channel to an air sample containing different concentrations of NO_2 via a tubing. The microfluidic channel is exposed to NO_2 with concentrations varying between 0 to 1 ppmV to cover the need of environmental monitoring.

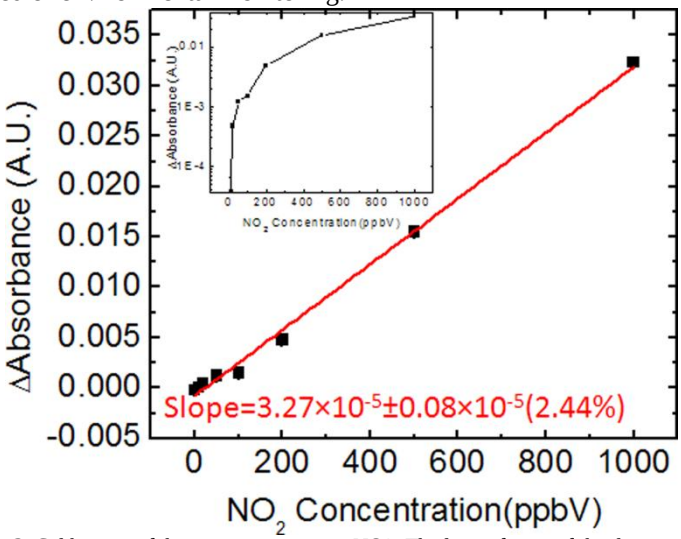

Fig. 3. Calibration of the sensor response to NO2. The linear fitting of the data gives a sensitivity of (3.27 ± 0.08) × 10^{-5} (2.44%). The inset is the calibration curve in log scale.

Fig. 3 plots the absorbance change determined with equation (1) vs. analyte concentration, showing a linear response to NO_2 over a wide dynamic range. These data are taken on the same microfluidic channel by applying equation (9) over the entire channel. The noise level of the absorbance is 10^{-4} over a period of ~30 mins, which determines a sensitivity of 50 ppbV·min, and allows detection of 10 ppb NO_2 in 5 minutes of sampling. This detection limit meets the needs of most environmental monitoring and industry safety

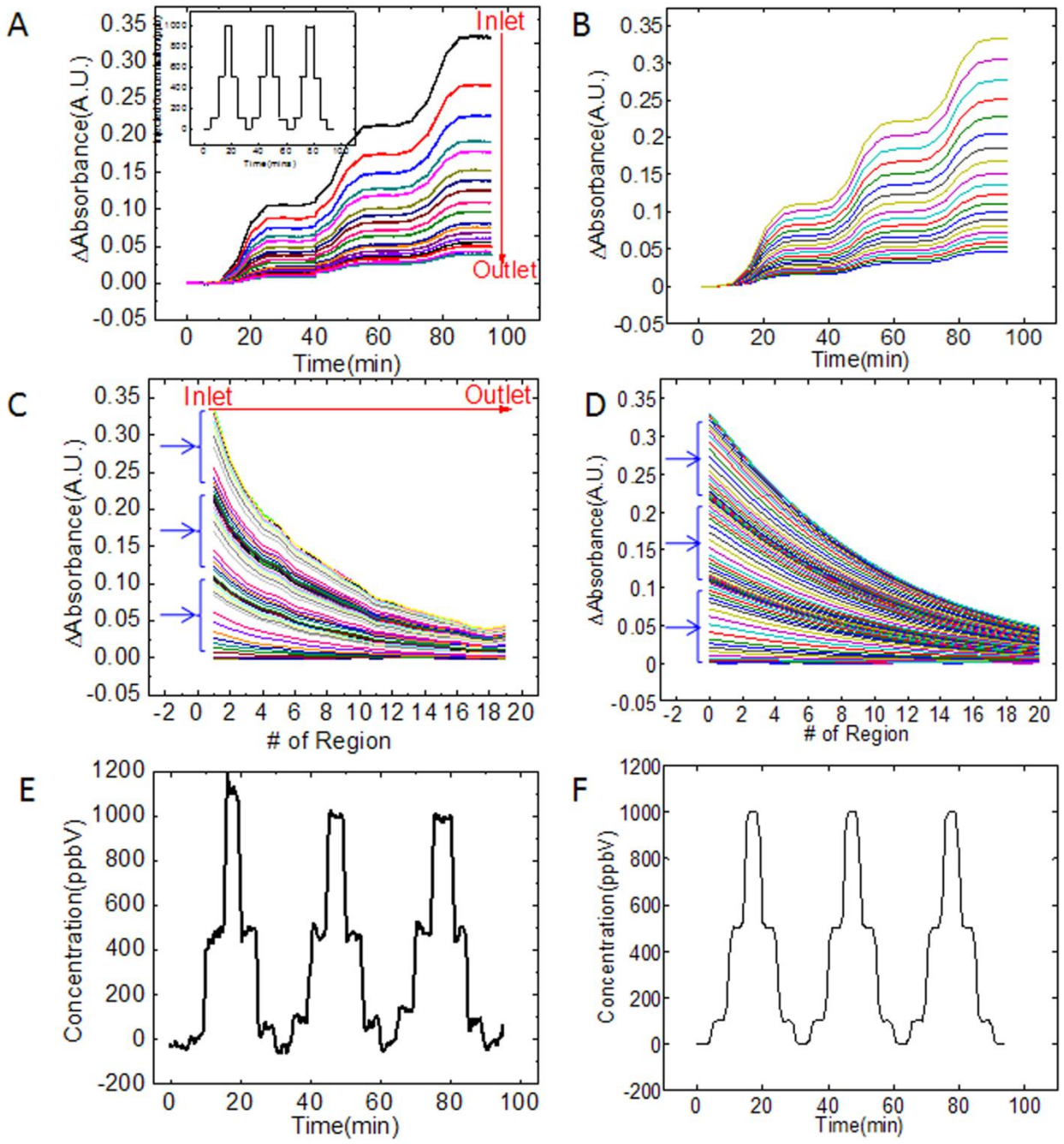

Fig. 4. Measured A) and simulated B) absorbance changes vs. time at different regions along the channel. Different colors represent different regions. The inset in A) is the injected NO2 concentration profile. For each concentration, the injecting time is 5 minutes. Measured C) and simulated D) absorbance changes along the channel at different times. Different colors represent different times. Measured E) and simulated F) concentration profiles

applications. The lifetime of the sensor is determined by the reaction capacity, which was calculated to be 1.8 ppmV·hr by integrating the analyte concentration over time until color saturation. This indicates the sensor can last for 18 hours for a continuous exposure to 100 ppbV of NO_2. This lifetime is long enough to monitor a person's exposure continually for a working day.

To further validate the microfluidic-colorimetric detection, we measure the color pattern along the channel, and its time evolution upon exposure to a range of concentrations of NO_2. As shown in the inset of fig. 4A, the concentration steps up from zero to 100 ppbV, 500 ppbV, and 1000 ppbV sequentially, and then steps down to 500 ppbV, 100 ppbV, and zero. At each step, the concentration is held constant for 5 mins. This process is repeated three times. Fig. 4A shows the absorbance change vs. time at multiple locations along the channel (solid lines with different colors), where the three large steps correspond to the three sample injection cycles. It also shows that although the inlet shows the largest absorbance change, other regions along the channel also

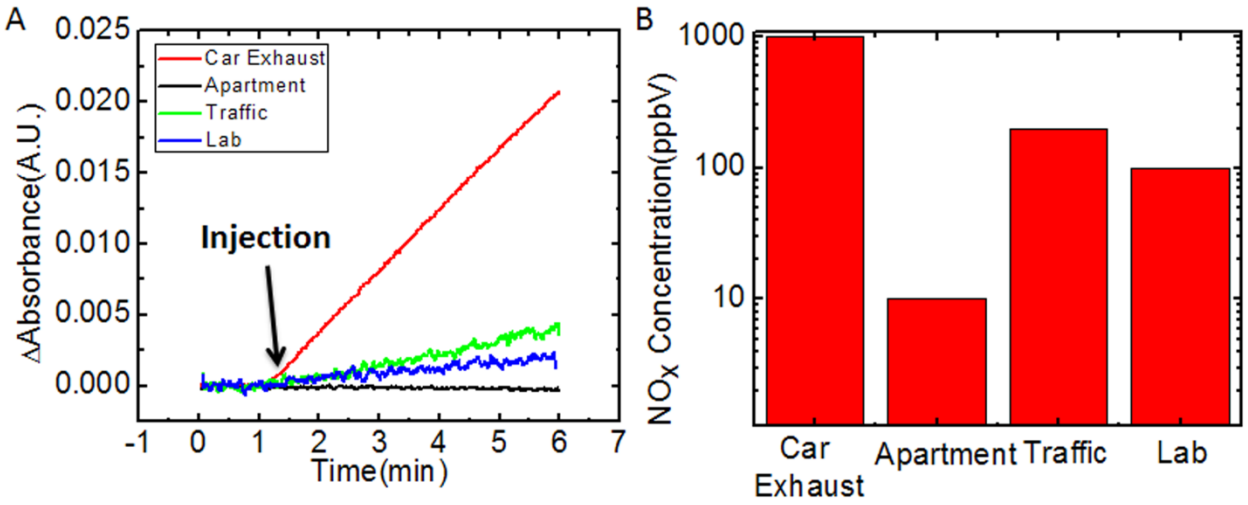

Fig. 5. A) Absorbance change of the sensor when exposed to different gas samples. B) NOx level of different sources.

displays a similar absorbance change pattern. Fig. 4C plots the absorbance variation along the channel at different times, showing more clearly different reaction rates along the entire channel. Note the curves in fig. 4C are obtained with equal time interval, but they are not equally spaced. In fact, they can be divided into three groups based on the spacing (see arrows in fig. 4C). The large spacing corresponds to the fastest change in the absorbance, which is due to a sample injection cycle.

Although both figures 4A and C contain analyte concentration information, the best way to extract the analyte concentration of the sample is to plot $\frac{1}{k(\Delta A_{\max} - \Delta A)} \frac{d\Delta A}{dt}$ over the channel. Fig. 4E shows such plot, which reproduces the analyte concentration variations. We have carried out theoretical simulations of the processes using the same inlet concentration profile as the experiments and estimated binding sites concentration (n_0 = 250 mol·m^{-3}). Figures 4B, D and F show the corresponding simulation results. The absorbance change and the concentration profile are obtained using equations (7) and (9). The amplitudes of the simulation data are adjusted by multiplying a constant. The simulated results are in excellent agreement with the experimental data.

C. Field tests

We performed field tests by sampling air at several locations, including apartment, car exhaust, a busy road, and laboratory, where NO_x concentrations vary over orders of magnitude (**Fig. 5**). Clean air was first introduced to establish baseline and the gas sample is then connected to the system (**Fig. 5A**). The NO_x concentration is calculated from equation (9). The NO_x level of the apartment was found to be lower than 10 ppbV, suggesting the indoor air had no significant NO_x. In contrast, the NO_x level in the laboratory was found to be ~100 ppbV. The traffic air sampled at a busy road in Tempe, AZ, during rush hour showed a high level of NO_x, ~200 ppbV. The air sampled directly from the car exhaust had an extremely high NO_x level of 1 ppmV. These field tests were preliminary and not meant for a thorough study of air quality, but it demonstrates that the microfluidic-colorimentric detection can provide continuous monitoring of air quality of microenvironments. The miniaturized size, and the unprecedented temporal and spatial resolution are expected to provide epidemiologists and environmental scientists a new tool to monitor personal air pollution exposures levels and to study sources and transport mechanism of air pollutants.

IV. Conclusion

A microfluidic-colorimetric approach was developed to overcome the longstanding difficulties, including irreversibility, slow recovery, and limited lifetime that are inherent to the conventional colorimetric sensors. These difficulties prevent the use of the colorimetric sensor for fast and continuous monitoring of air pollution. To establish the microfluidic-colorimetric approach, theoretical simulations and analytical experiments are carried out and compared with each other. The results show that the approach can prolong the sensor's lifetime without sacrificing its sensitivity. In the case of NO_x detection, the sensor can continuously monitor air quality over 18 hours with a detection limit of 50 ppbV·min. The detection principle can be extended to the detection of other analytes. Preliminary field tests have also been carried out to demonstrate the sensor's capability of monitoring NO_x level in a variety of real environments. The small dimension of the sensor and low power consumption promise a miniaturized sensor for monitoring personal exposure to microenvironment, and for mapping local air pollution for environmental protection and studies.

References

[1]B. Son, *et al.*, "Estimation of occupational and nonoccupational nitrogen dioxide exposure for Korean taxi drivers using a microenvironmental

model," *Environmental Research*, vol. 94, pp. 291-296, Mar 2004.

[2] H. Papke and H. Papen, "Influence of acid rain and liming on fluxes of NO and NO2 from forest soil," *Plant and Soil*, vol. 199, pp. 131-139, Feb 1998.

[3] C. Nevison and E. Holland, "A reexamination of the impact of anthropogenically fixed nitrogen on atmospheric N2O and the stratospheric O-3 layer," *Journal of Geophysical Research-Atmospheres*, vol. 102, pp. 25519-25536, Nov 1997.

[4] S. A. Abdul-Wahab, *et al.*, "Using the integrated empirical rate-reactive plume model in assessment of the potential effects of Shuaiba Industrial Area NOx plumes on photochemical smog concentrations," *Process Safety and Environmental Protection*, vol. 81, pp. 363-374, Sep 2003.

[5] A. Holmen, *et al.*, "Frequency of patients with acute asthma in relation to ozone, nitrogen dioxide, other pollutants of ambient air and meteorological observations," *International Archives of Occupational and Environmental Health*, vol. 69, pp. 317-322, May 1997.

[6] "Health Aspects of Air Pollution with Particulate Matter, Ozone and Nitrogen Dioxide," Report on a WHO working group, Bonn, Germany13-15 January 2003.

[7] "Final revisions to the national ambient air quality standards for nitrogen dioxide," EPA2010.

[8] A. Lozano, *et al.*, "Air Quality Monitoring Network Design to Control Nitrogen Dioxide and Ozone, Applied in Granada, Spain," *Ozone-Science & Engineering*, vol. 33, pp. 80-89, 2011.

[9] *GE Analytical Instruments - Sievers nitric oxide analyzer (NOA) 280i*. Available: http://www.globalspec.com/FeaturedProducts/Detail/GEAnalyticalInstruments/Sievers_Nitric_Oxide_Analyzer_NOA_280i/45831/0

[10] J. K. Robinson, *et al.*, "Luminol/H2O2 chemiluminescence detector for the analysis of nitric oxide in exhaled breath," *Analytical Chemistry*, vol. 71, pp. 5131-5136, Nov 1999.

[11] N. A. Rakow and K. S. Suslick, "A colorimetric sensor array for odour visualization," *Nature*, vol. 406, pp. 710-713, Aug 2000.

[12] A. Prabhakar, *et al.*, "Ultrasensitive Detection of Nitrogen Oxides over a Nanoporous Membrane," *Analytical Chemistry*, vol. 82, pp. 9938-9940, Dec 2010.

[13] J. Douglas and T. F. Russell, "Numerical-methods for convection-dominated diffusion-problems based on combining the method of characteristics with finite-element or finite-difference procedures," *Siam Journal on Numerical Analysis*, vol. 19, pp. 871-885, 1982.

[14] H. A. Stone, "A simple derivation of the time-dependent convective-diffusion equation for surfactant transport along a deforming interface," *Physics of Fluids a-Fluid Dynamics*, vol. 2, pp. 111-112, Jan 1990.

[15] H. Bruus, *Theoretical microfluidics*, 2003.

[16] G. Latini, *et al.*, "Thermophysical properties of greenhouse gases thermal conductivity and dynamic viscosity as function of temperature and pressure," *Energy Conversion and Management*, vol. 37, pp. 1291-1296, Jun-Aug 1996.

[17] W. R. Hwang and S. G. Advani, "Numerical simulations of Stokes Brinkman equations for permeability prediction of dual scale fibrous porous media," *Physics of Fluids*, vol. 22, Nov 2010.

[18] H. Davarzani, *et al.*, "Experimental measurement of the effective diffusion and thermodiffusion coefficients for binary gas mixture in porous media," *Chemical Engineering Science*, vol. 65, pp. 5092-5104, Sep 2010.

[19] Y. Sato, *et al.*, "Solubilities and diffusion coefficients of carbon dioxide and nitrogen in polypropylene, high-density polyethylene, and polystyrene under high pressures and temperatures," *Fluid Phase Equilibria*, vol. 162, pp. 261-276, Aug 1999.